JOURNAL OF AIRCRAFT
Vol. 44, No. 1, January–February 2007

Riveting Process Induced Residual Stresses Around Solid Rivets in Mechanical Joints

Calvin Rans* and Paul V. Straznicky†
Carleton University, Ottawa, Ontario K1S 5B6, Canada
and
René Alderliesten‡
Delft University of Technology, 2629 HS Delft, The Netherlands

DOI: 10.2514/1.23684

The interference fit provided by solid rivets introduces a residual stress field beneficial to the fatigue life of riveted joints. Evolution in riveting technology has led to force-controlled riveters which provide greater consistency over the rivet installation process and the resulting residual stress field. By reexamining the rivet installation process and its effects on the formation of residual stresses, the fatigue benefits of rivets could be further exploited. Using a 3-D finite element model, installation of universal and countersunk rivets in monolithic aluminum sheet has been studied. Aspects of accepted riveting practice, including the degree of rivet flushness and the rivet squeeze force were found to play significant roles in the formation of residual stresses. Residual stresses beneath the rivet head were also found to be influenced primarily by through-thickness compression of the joined sheets during riveting, challenging the traditional analogy of riveting to radial expansion processes.

Nomenclature

D	=	driven rivet head diameter
D_o	=	uninstalled rivet shank diameter
F_{Sq}	=	rivet squeeze force
h	=	installed rivet tail height
h_o	=	uninstalled rivet tail height
R	=	rivet hole radius
t	=	sheet thickness
ε_r	=	radial strain
ε_θ	=	hoop strain
σ_r	=	radial stress
σ_y	=	yield stress
σ_{zz}	=	through-thickness stress
σ_θ	=	hoop stress

I. Introduction

MECHANICAL fastening is one of the major methods for joining airframe structural components and its use will continue in the foreseeable future despite a number of disadvantages and alternatives such as welding and bonding. Localized load transfer at discrete fastener locations causes stress concentrations which increase susceptibility to fatigue. Current practices for design against fatigue rely heavily on simplified analytical models, design "rules of thumb," and verification testing. The rivet installation process and its implications on the fatigue performance of riveted joints will be the focus of this paper.

Rivet installation is typically governed by design rules of thumb and is generally not considered a design variable. Developments in riveting technology and the advent of force-controlled and fully automated riveting machines, however, have improved the consistency of rivet installation, providing the opportunity to include its influence on fatigue at the design stage. This influence is well understood on a qualitative level. Expansion of the rivet shank during installation produces an interference that results in a residual stress field around the rivet hole. The nature of this residual stress field and its impact on subsequent joint loading plays an important role in the nucleation and growth of cracks in the vicinity of the rivet hole. Furthermore, the final geometry of an installed rivet influences the clamping and bending constraints provided by the rivet. Fretting damage and the potential for fretting-induced crack initiation at faying joint surfaces are highly dependent on the materials, clamping force, and the constraint provided by the installed rivet. The geometry of the manufactured and driven rivet heads also influences the location of peak bending stress due to rivet rotation, a prime location for crack initiation. A quantitative understanding of these factors is essential for design optimization of riveted joints.

A detailed investigation into the influence of rivet installation force (squeeze force) completed by Müller [1] demonstrated that the fatigue life of riveted joints could be increased tenfold by increasing the squeeze force. Since these findings, several finite element (FE) studies have been undertaken in an attempt to further understand this relationship [2–7]. These studies, however, have been limited to investigating the influence of the rivet squeeze force in the context of single combinations of rivet type and sheet material. The influence of rivet type, in conjunction with the rivet squeeze force, on residual stress distribution is still largely unknown.

Motivated by the need for greater understanding of the rivet installation process, a 3-dimensional FE model was developed to study the installation process of 2117-T4 aluminum rivets in monolithic 2024-T3 aluminum sheets. Only a single sheet thickness and rivet diameter were considered. Within this scope, the influence of the following riveting parameters was studied: 1) rivet squeeze force, 2) universal vs countersunk rivets (MS20470AD4-4 and NAS1097AD4-4, respectively), and 3) rivet flushness before installation.

Each of these parameters is first discussed in the context of traditional design rules of thumb and riveting practice and examined in the context of force-controlled riveting.

II. Finite Element Model

A. Model Description

The configuration chosen for the finite element model consisted of two 1.0 mm thick 2024-T3 plates joined at their centers by a single 3.2 mm diameter 2117-T4 aluminum rivet. Installation of universal head (U.S. military specification MS20426AD4-4) and reduced-

Received 6 March 2006; revision received 24 May 2006; accepted for publication 9 June 2006.

*Ph.D. Student, Department of Mechanical and Aerospace Engineering.
†Professor, Department of Mechanical and Aerospace Engineering.
‡Professor, Faculty of Aerospace Engineering.

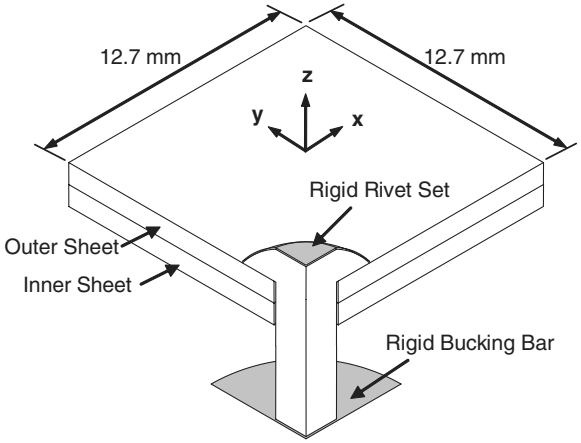

Fig. 1 Schematic of the 3-D FE model.

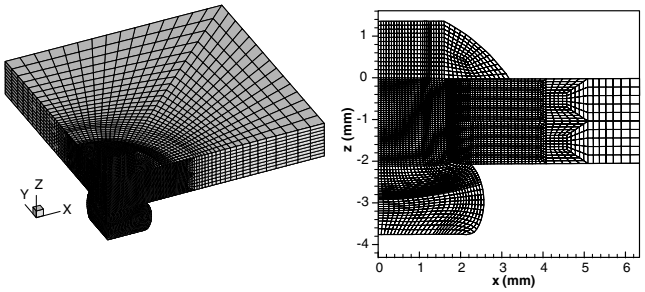

Fig. 2 Typical mesh density shown for universal rivet case in the deformed configuration.

depth countersunk head (NAS1097AD4-4) rivets of length 6.4 mm were investigated. The 3-dimensional quarter symmetry model used in this study is shown schematically in Fig. 1. The use of 3-dimensional finite element techniques was chosen over more simplified axisymmetric finite element techniques to facilitate future extensions of the model [8].

A typical mesh for the universal head rivet case is shown in Fig. 2. Mesh generation and additional preprocessing steps were performed using the software package ETA/FEMB v28 [9] while solutions for the models were obtained using the nonlinear explicit finite element code LS-DYNA v970 [10]. Eight-node single-point integration brick elements (ELFORM = 1) were used to represent the rivet and plates. Rivet tools were defined as rigid surfaces using 4-node shell elements. The use of single-point integration brick elements introduces the potential for zero-energy deformation modes known as hourglass modes, where element deformation results in no straining of the element. The use of higher-order elements avoids the potential for hourglassing; however, such elements are computationally more expensive and less suited to large-deformation problems due to their sensitivity to element distortion. To allow the use of single-point integration brick elements and avoid the occurrence of hourglass deformation modes, type-6 stiffness based hourglass control options in LS-DYNA were employed.

Symmetry boundary conditions were applied along the two quarter symmetry and two plate periphery planes. The outer and inner plates were further constrained by restricting motion of the nodes along the periphery of their free surface in the rivet axis direction. Motion of the rigid riveting tools was constrained by fixing the position of the rivet set and restricting the rivet bucking bar to translation along the rivet axis (Fig. 3). All other constraints were provided through contact definitions specified using the segment-based automatic contact options in LS-DYNA. Automatic contact allows the user to define contacting pairs by parts or groups of parts without the need for explicitly defining contact elements. LS-DYNA automatically generates contact elements as needed during the simulation to resolve contact between the defined contact pair. The current model included four contact pairs defining contact between

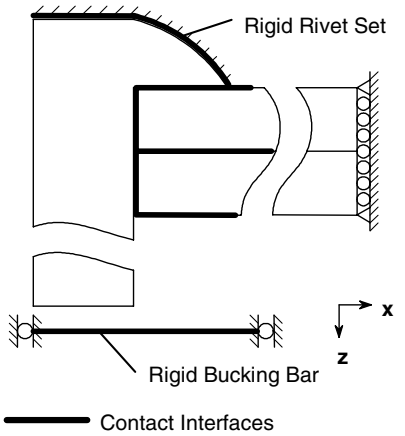

Fig. 3 2-D schematic of FE boundary conditions.

the rivet and each of the rivet tools, between the rivet and the plates, and along the faying surface between the inner and the outer plate. A coefficient of friction of 0.18 was specified for each of the contact interfaces [5].

Installation of the rivet was simulated by applying a ramp load–unload cycle to the rigid bucking bar. Because of the nature of explicit time integration schemes, two dwell periods were included after the loading and unloading phases to allow the system to fully come to rest. A residual squeeze force of 2 N was prescribed at the end of the unloading phase to prevent oscillations in the simulation from forming due to a break in contact between the rivet and riveting tools, thereby minimizing the required dwell time. Five squeeze forces were considered in this study: 1000, 1500, 2000, 2500, and 3000 lbf (4.4, 6.8, 8.9, 11.1, and 13.3 kN, respectively). Quasistatic assumptions were applied and simulation time was scaled to minimize processing time.

B. Material Modeling

Nonlinear material models for both the 2024-T3 aluminum plate and the 2117-T4 aluminum rivet materials were required for the present investigation. Although the plastic behavior of the 2024-T3 plate is well documented [11], relatively few studies into the large strain behavior of 2117-T4 rivet material have been conducted. A review of the literature found two separate studies which resulted in suitable nonlinear material models for 2117-T4. The first model, developed by Szolwinski and Farris [7], used compression tests on billet samples extracted from actual rivet shanks. The experimental data, however, was limited to a strain range of $0.02 \leq \varepsilon_{\text{true}} \leq 0.10$ bringing into question the validity of extrapolating the model for higher strains which would be present during rivet forming. The second model, developed by de Rijck [12], used experimental driven rivet head geometries and simplified analytical models for the deformation of the rivet shank; however, the model became available only after the current study was nearly complete. Good agreement was found between the two models over the strain range of Szolwinski's experimental data; however, a lower strain hardening behavior was observed in the extrapolated region of Szolwinski's

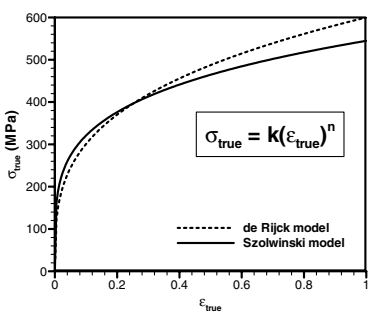

Fig. 4 Comparison of 2117-T4 rivet material model true stress-strain curves.

Table 1 Summary of material models used for the rivet and plate materials

Material model parameter	Value
2117-T4 (power law plasticity) [7]	
Elastic modulus, E	71.7 GPa
Strength coefficient, k	544 MPa
Hardening exponent, n	0.23
Poisson ratio, ν	0.33
2024-T3 (power law plasticity) [11]	
Elastic modulus, E	72.4 GPa
Strength coefficient, k	530 MPa
Hardening exponent, n	0.10
Poisson ratio, ν	0.33

model (Fig. 4). Despite the differences in the material models, FE simulations repeated using de Rijck's model showed negligible difference in rivet deformation and resulting residual stress state in the 2024-T3 plates; thus only results from the original simulations utilizing Szolwinski's 2117-T4 rivet material model will be presented. A summary of the material models used is given in Table 1.

C. FE Model Verification

Verification of the finite element model was not a trivial task. The residual stress results of interest are hidden beneath the manufactured and driven rivet heads, making most experimental stress analysis techniques unfeasible. Stresses and strains beyond the rivet head can easily be determined experimentally; however, this is not an adequate measure for verifying the performance of the model underneath the rivet head where stress and strain magnitudes and gradients can be greater by an order of magnitude or more. To verify the performance of the finite element model in the critical region beneath the rivet head, the model was adapted to simulate the cold expansion process. The radial expansion mechanisms for forming residual stress during riveting and cold expansion are analogous; however, cold expansion is a simpler process for which analytical models are available [13–16]. The finite element results were found to agree well with such analytical models, improving confidence in the present model. Further details of the cold expansion simulations can be found in another paper by the present authors [17].

Although most experimental measurement techniques cannot provide adequate results for verification of the FE model, methods such as neutron diffraction can determine the residual strain state beneath the rivet head. The exorbitant costs of this technique made this method beyond the resources of this study. However, a similar neutron diffraction study completed by Li et al. [18] was available. Modifications to the current FE model geometry were implemented to represent the MS20426AD8-9 rivet and 2.0 mm thick 2024-T3 sheets used in the experimental study. Figure 5 shows a comparison of the FE model results to the neutron diffraction data. The residual strain magnitudes agree well with the FE model, with some discrepancies occurring near sharp peaks in strain ($x = 4$–5 mm). Capturing these sharp peaks using the neutron diffraction method becomes difficult due to the required gauge volume over which the residual strain is determined for each data point. This neutron

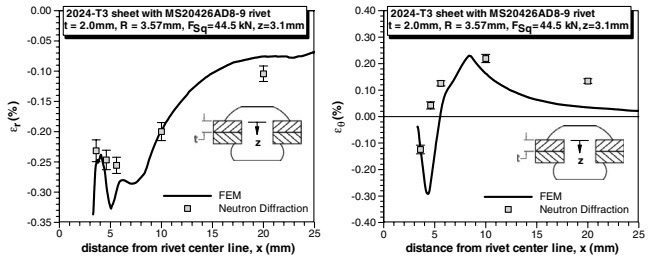

a) b)

Fig. 5 Comparison of FE residual strains to neutron diffraction data [18]: a) radial strain; b) hoop strain.

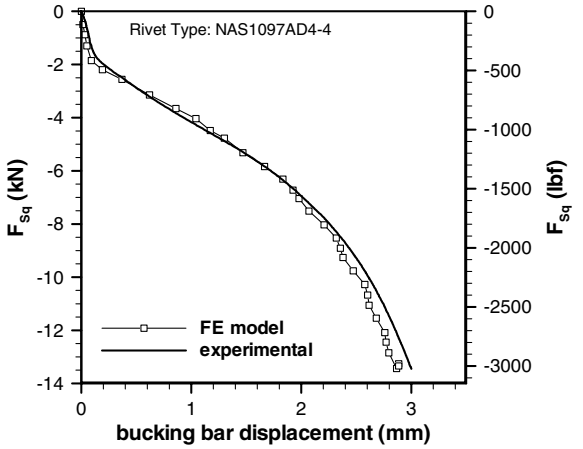

Fig. 6 Comparison of FE and experimental bucking bar force-deflection curves.

diffraction study used a gauge volume of 1 mm^3. Further details on the exact geometries of these gauge volumes can be found in [18].

Another common benchmark that has been used in previous rivet forming studies is the load-deflection behavior of the rivet bucking bar during rivet installation [4–7]. The load-deflection behavior of the bucking bar was obtained experimentally using a MTS servohydraulic test frame fitted with standard riveting tools and is shown in Fig. 6 alongside the FE results. Good agreement is observed with the experimentally obtained curve with less than a 5% error, verifying the stiffness and plasticity of the rivet material model.

Although no direct verification of the results for the FE model in its configuration used for this study could be made, much effort has been placed in testing and validating indirectly all the aspects of the FE model. From the results of these efforts, a high degree of confidence in the performance and results of the FE model has been established.

III. Results

For presentation purposes, in-plane and thickness positions within the sheets have been normalized by the rivet hole radius and sheet thickness, respectively. Stress results have also been normalized by the yield stress of the 2024-T3 sheets.

The degree of hole expansion resulting over the range of rivet squeeze forces for the universal and countersunk rivet cases is shown in Fig. 7. Two additional dash-dot-dotted lines are plotted in Fig. 7b illustrating the divergence in the level of hole expansion at high squeeze forces between countersunk rivets that are initially perfectly flush and rivets that protrude 0.07 mm above the outer sheet. Experience has shown that a small protrusion of the rivet head above the sheet surface during rivet installation has a beneficial effect on fatigue performance of riveted splices, likely due to improved hole filling of the conical recess of the countersunk sheet. Standard riveting practice also dictates that countersink depths should be produced such that the height of the protrusion falls in the range of 0.01–0.2 mm [1]. Results for the perfectly flush countersunk rivet

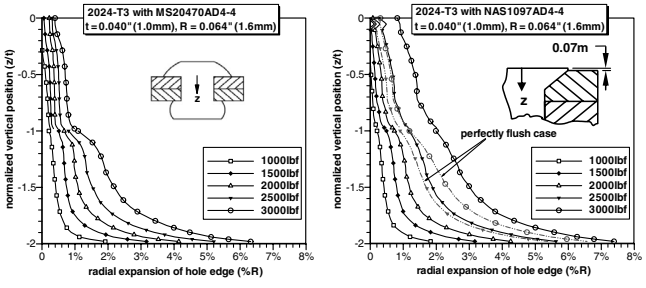

a) b)

Fig. 7 Variation of rivet hole radial expansion levels with rivet squeeze force: a) universal rivet case; b) countersunk rivet case.

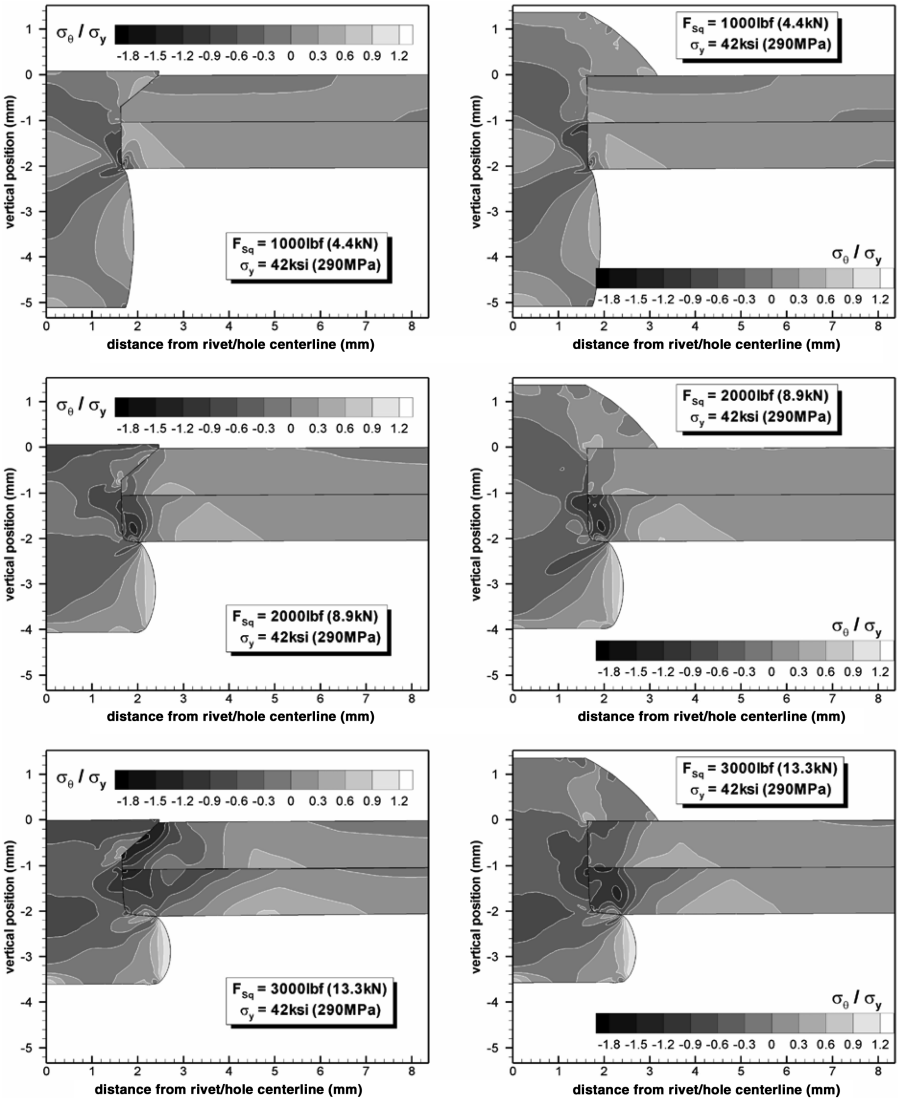

Fig. 8 Residual hoop stress distributions for countersunk and universal rivets installed with 4.4, 8.9, and 13.3 kN squeeze forces.

case are shown here for comparative purposes. All other references to countersunk rivet results refer to the 0.07 mm protruding rivet head case unless otherwise stated.

Contour plots comparing the residual hoop stress distributions for countersunk and universal rivets are shown in Fig. 8. The regions of compressive hoop stress near the rivet hole are of primary interest due to their positive influence on prolonging crack nucleation and reducing crack growth rates. Knowledge of residual stress distributions along the faying joint surfaces is important as they are most adversely affected by fretting and tensile secondary bending stresses under joint loading conditions, making them a likely location for crack initiation. Line plots of the residual hoop stress distributions along the inner and outer sheet faying surfaces are shown in Fig. 9.

The resulting driven rivet head diameter ratio (D/D_o) for each rivet squeeze force is shown in Fig. 10. With the exception of the lowest squeeze force examined, all of the rivet squeeze forces resulted in rivet installations that would be deemed acceptable using the design rule of thumb dictating that D/D_o should fall within the range of 1.3–1.8 [1]. The variations in residual stresses observed in the FE simulations are thus plausible in a single joint using this rule of thumb to assess rivet quality.

IV. Discussion

A. Formation of Residual Stresses

The formation of residual stresses during riveting is often likened to cold expansion processes whereby large radial stresses plastically deform the material surrounding a fastener hole. Elastic springback of the bulk material then compresses the plastically deformed material producing the residual stress state. This mechanism was indeed observed in the FE simulations. However, through-thickness compression of the joint sheets during rivet installation was also found to play a significant role in the formation of residual stresses underneath the rivet head.

A typical residual hoop stress distribution observed in the FE models is shown in Fig. 11 and has been divided into four zones for discussion purposes. Zones 1–3 correspond to the regions surrounding the rivet which undergo plastic deformation during riveting while zone 4 is the region of elastic deformation. Within the plastic region, zones 1 and 2 experience large through-thickness compressive stresses (often exceeding the radial compressive stresses by a factor of 2) resulting from part of the rivet squeeze force being transmitted through the driven rivet head into the underlying sheets (Fig. 12). The importance of this through-thickness stress on the formation of residual stresses is often overlooked in discussions on riveting; however, it contributes to the plastic deformation of the sheet beneath the rivet head and resulting residual stress state. This is clearly seen in Fig. 11 where a steeper gradient in residual hoop stress is generated in the region affected by the high through-thickness stresses, producing higher magnitude compressive stresses near the fastener hole. Zone 3 lies beyond the driven rivet head and does not experience large through-thickness stresses. The formation of residual stresses in this region closely follows the cold expansion analogy, and the residual stress magnitudes and gradients showed

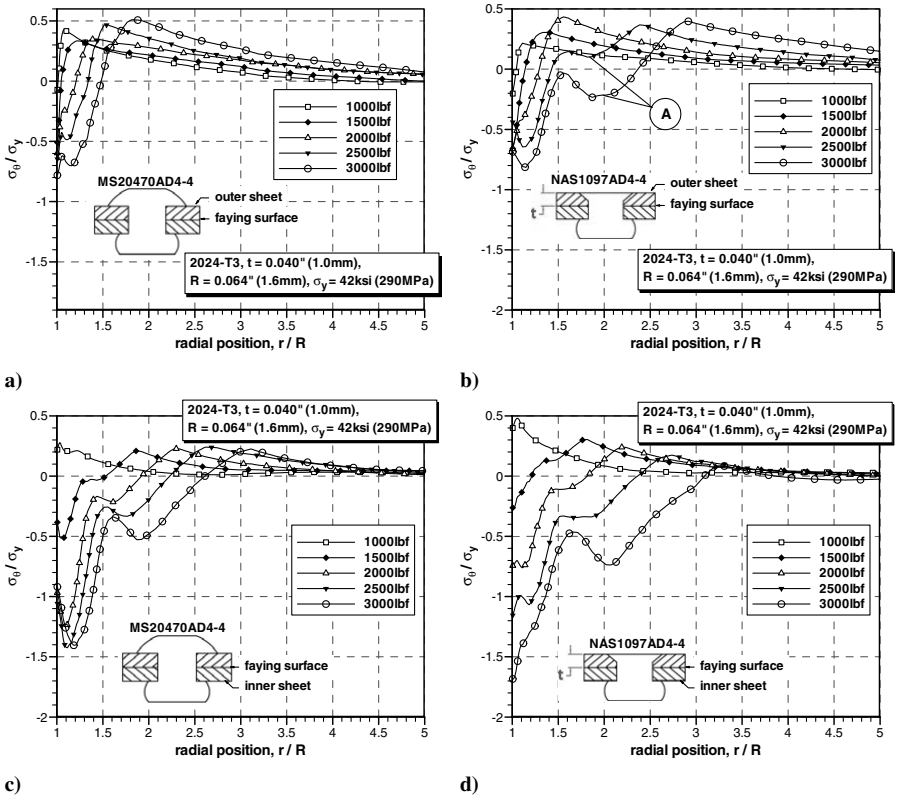

Fig. 9 Influence of rivet squeeze force on faying surface residual hoop stress: a) outer sheet with universal rivet; b) outer sheet with countersunk rivet; c) inner sheet with universal rivet; d) inner sheet with countersunk rivet.

similar trends to analytical and numerical cold expansion models examined by the present authors in another paper [17].

The region and magnitude of the compressive residual hoop stresses was found to increase with rivet squeeze force. Although no limit to this increase was identified, experience has shown that larger driven rivet head dimensions associated with larger squeeze forces tend to shift the crack nucleation location away from the fastener hole, negating the benefit of the residual compressive stresses. Under the footprint of the larger driven rivet head dimensions, peak secondary bending stresses resulting from rivet rotation flow around the fastener hole, driving the shift in crack nucleation location. This influence of rivet geometry and rivet squeeze force on secondary bending will be investigated further in future studies.

B. Countersunk Rivet Flushness

The importance of the degree of rivet flushness before rivet installation on fatigue performance is alluded to by a standard riveting practice regarding the range of acceptable heights the countersunk rivet head is permitted to protrude above the countersunk sheet. This practice ensures that the countersunk depth of the sheet does not exceed the height of the countersunk rivet head, which would result in poor hole filling within the countersunk sheet during riveting. Additionally, too deep a countersink would minimize the rivet-sheet contact during riveting, reducing the benefit of through-thickness compressive stresses described above. Previous FE studies investigating rivet installation have opted for simulating either idealized perfectly flush countersunk rivets [1,3,5] or countersunk rivets with a small initial protrusion above the outer sheet [4]. However, none have compared the relative performance of the two cases. Both cases have been considered in this study and will be discussed.

Comparison of results for the two flushness cases from this study shows that the degree of rivet flushness influences the amount of hole expansion and formation of residual stresses at high squeeze forces,

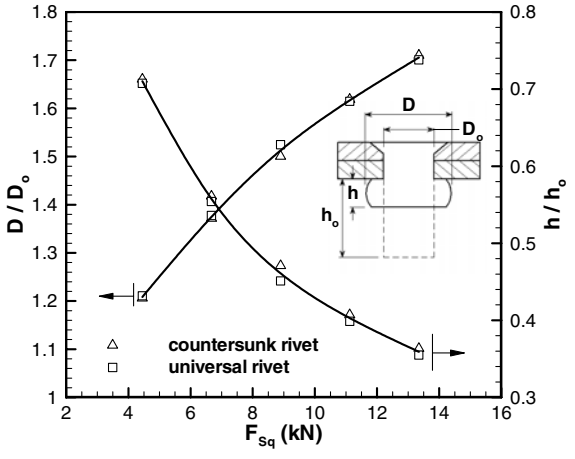

Fig. 10 FEM comparison of driven rivet head geometry and rivet squeeze force.

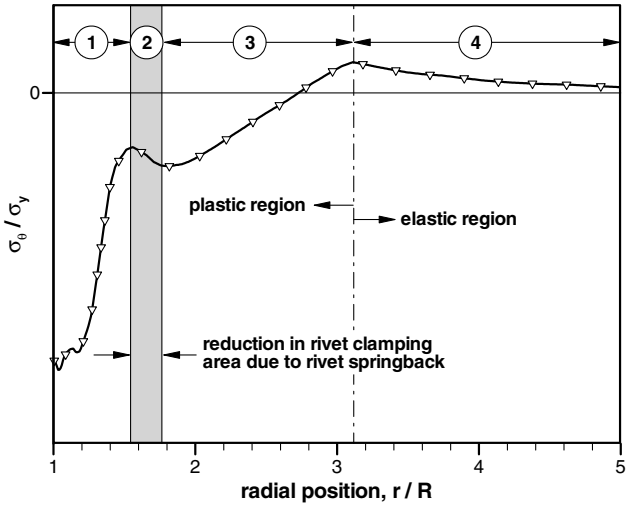

Fig. 11 Schematic of residual hoop stress distribution.

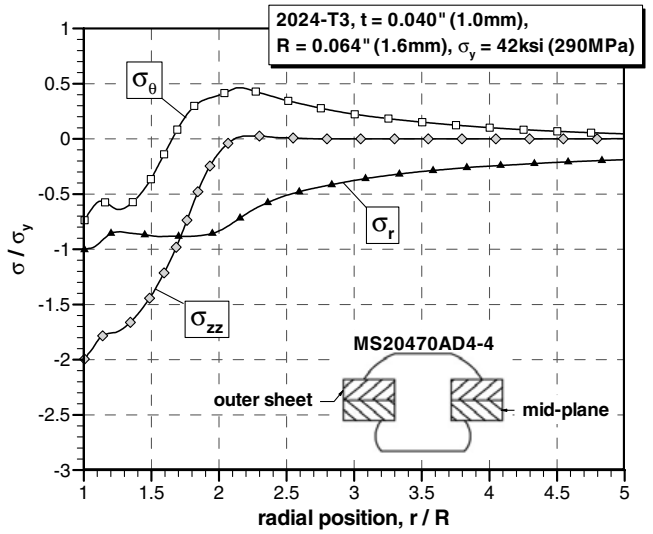

Fig. 12 Outer sheet midplane stresses under maximum applied squeeze force.

but negligible influence at lower squeeze forces. This is illustrated in Fig. 7b where the degrees of radial expansion for the two cases diverge for squeeze forces greater than 2000 lbf. This squeeze force also corresponds to the point at which the driven rivet head diameter exceeds that of the countersunk rivet head. At these higher squeeze forces, frictional slip occurs causing the countersunk sheet to slide up the countersunk rivet head and expand through a wedging action (wedge expansion). The addition of this expansion mechanism increases the radial pressure between the rivet and the countersunk sheet, resulting in the radial stress dominated region of plasticity (zone 3, as described in Sec. IV.A) indicated by balloon A in Fig. 9b. This is further illustrated by the residual hoop stress distributions for both countersunk rivet cases resulting from a 3000 lbf rivet squeeze force shown in Fig. 13. The higher magnitude and larger region of residual compressive stress associated with wedge expansion of the countersunk rivet head would be beneficial to the fatigue performance of the countersunk sheet.

In addition to the wedge-expansion mechanism, a protruding rivet head localizes the through-thickness compressive stress resulting from the squeeze force. For the perfectly flush case, the rivet set contacts both the rivet and the surrounding outer sheet, distributing the rivet squeeze force over a larger area. A small degree of rivet protrusion eliminates contact between the rivet set and the outer

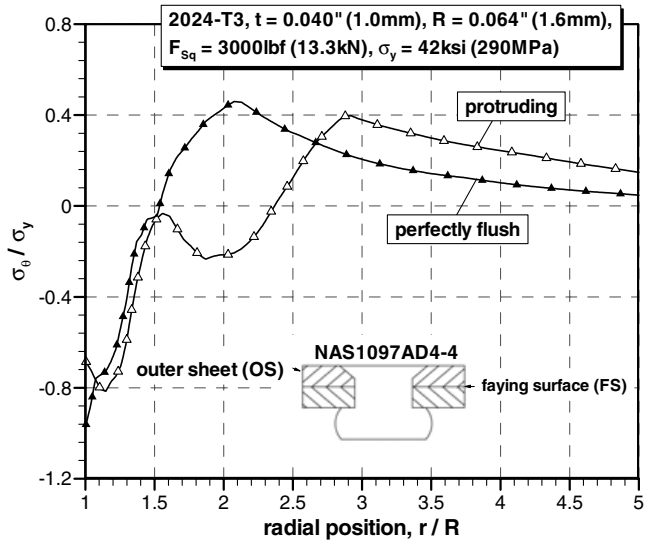

Fig. 13 Comparison of outer sheet faying surface residual hoop stress distribution for perfectly flush and 0.07 mm protruding countersunk rivet.

sheet, localizing the transfer of force into the sheets to the conical contact region between the rivet and outer sheet. This contributes to the formation of residual stresses beneath the rivet head. However, it would not provide as great a contribution to the formation of zone 3, as shown in Fig. 13, as the wedge-expansion mechanism.

Existing fatigue data support the influence of rivet flushness. Experimental studies carried out by Müller [1] found a correlation between the amount of rivet head protrusion, rivet squeeze force, and a shift in fatigue cracking from the countersunk to noncountersunk sheet in riveted splices containing NAS1097 style countersunk rivets. He attributed this effect to changes in secondary bending resulting from a permanent curvature (or *imperfection* as it was called) formed by bending of the inner and outer sheets around the protruding countersunk rivet head at high squeeze forces. The increase in compressive hoop stresses within the countersunk sheet resulting from the wedge-expansion mechanism could also contribute to this shift in fatigue cracking. Additionally, the onset of formation of an imperfection was also observed by Müller to occur when the driven rivet head exceeded the countersunk rivet head, which also agrees with the onset of the wedge-expansion mechanism in the present study.

Li and Shi [4] also investigated the residual stress state resulting from the installation of a countersunk rivet that protruded 0.07 mm above the sheet surface; however, there was no evidence of the wedge expansion described above. Several key differences in their model could have contributed to this finding. First, Li and Shi considered a MS20426 style countersunk rivet, which has a larger countersunk head than the NAS1097 style considered in the current investigation. As a result, the driven rivet head diameter did not exceed the countersunk rivet head diameter in their simulations. Bending in the outer sheet associated with this event could be critical in initiating frictional slip between the outer sheet and countersunk rivet head. Second, the depth of the countersink was equal to the thickness of the outer sheet in Li and Shi's model. The absence of a cylindrical hole surface in the outer sheet removes the contribution of radial pressure along this surface to frictional slip.

C. Universal Versus Countersunk Rivets

Generally, the use of universal rivets results in an overall improvement in fatigue life over similar joints using countersunk rivets. It is often speculated that part of the reason for this improvement results from greater radial expansion of the cylindrical hole surface in the outer sheet of universal rivet joints compared to the conical hole surface in countersunk joints. This hypothesis, however, is not supported by the results of this study. Expansion levels in the outer sheet were identical for universal and countersunk rivets below the squeeze force threshold for the wedge-expansion mechanism and greater for countersunk rivets when wedge-expansion occurred (Fig. 7). Similarly, the resulting outer sheet residual compressive hoop stresses were nearly identical below the squeeze force threshold for wedge expansion and more favorable for the countersunk rivet case when wedge expansion occurred (Fig. 8). These results suggest that residual stresses do not play a significant role in the improved fatigue performance of universal rivet joints over countersunk rivet joints. It is believed that the disparity in fatigue performance between universal and countersunk rivet joints should be sought in other factors such as the added stress concentration due to the machined countersink, variations in secondary bending stress around the rivet head, and variations in bearing stress and load transfer related stress concentrations under joint loading conditions. Future extensions of the current FE model to simulate loading and unloading of a rivet in a splice are planned to confirm this hypothesis.

V. Conclusions

Knowledge of the residual stress field generated during the rivet forming process and an understanding of the rivet installation parameters that influence it are necessary to exploit the fatigue life potential of riveted joints. Using a 3-D finite element model, the installation of both universal and countersunk rivets in 2024-T3

aluminum was investigated. Based on the results of this model, the following conclusions can be made:

1) Large through-thickness stresses are generated in the joint sheets underneath the rivet head during rivet installation, contributing to plasticity within this region. Gradients and magnitudes of the resulting residual hoop stress field in this region are larger than those predicted by radial expansion models, highlighting the importance of these through-thickness stresses in riveted joints.

2) Increases in the rivet squeeze force result in larger regions and magnitudes in residual compressive hoop stresses. Within the current study, no limiting or optimum squeeze force has been identified. However, future studies are planned to investigate the influence of rivet installation in loaded splices and identify limits to the benefits of high squeeze forces.

3) The importance of the degree of flushness of countersunk rivets before installation was confirmed by the present investigation. Additionally, limited protrusion of the countersunk rivet head above the joint surface was found to result in expansion of the outer sheet through a wedging action at high rivet squeeze forces. This expansion mechanism may be related to the geometric ratio of the driven and manufactured rivet head. However, further investigation is required.

4) Universal rivets do not provide any significant increase in expansion of the outer joint sheet compared to countersunk rivets. In instances where the wedging expansion mechanism was present, countersunk rivets provide improved expansion and residual compressive tangential stresses in the outer joint sheet.

References

[1] Müller, R. P. G., "An Experimental and Analytical Investigation on the Fatigue Behaviour of Fuselage Riveted Lap Joints: The Significance of the Rivet Squeeze Force and a Comparison of 2024-T3 and Glare 3," Ph.D. Dissertation, Delft University of Technology, Delft, The Netherlands, 1995.

[2] Deng, X., and Hutchinson, J. W., "The Clamping Stress in a Cold-Driven Rivet," *International Journal of Mechanical Sciences*, Vol. 40, No. 7, 1998, pp. 683–694.

[3] Langrand, B., Deletombe, E., Markiewicz, E., and Drazetic, P., "Riveted Joint Modeling for Numerical Analysis of Airframe Crashworthiness," *Finite Elements in Analysis and Design*, Vol. 38, No. 1, 2001, pp. 21–44.

[4] Li, G., and Shi, G., "Effect of the Riveting Process on the Residual Stress in Fuselage Lap Joints," *CASI Journal*, Vol. 50, No. 2, 2004, pp. 91–105.

[5] Ryan, L., and Monaghan, J., "Failure Mechanism of Riveted Joint in Fibre Metal Laminates," *Journal of Materials Processing Technology*, Vol. 103, No. 1, 2000, pp. 36–43.

[6] Szolwinski, M. P., "The Mechanics and Tribology of Fretting Fatigue with Application to Riveted Lap Joints," Ph.D. Dissertation, Purdue Univ., West Lafayette, IN, 1998.

[7] Szolwinski, M. P., and Farris, T. N., "Linking Riveting Process Parameters to the Fatigue Performance of Riveted Aircraft Structures," *Journal of Aircraft*, Vol. 37, No. 1, 2000, pp. 130–137.

[8] Rans, C. D., Alderliesten, R. C., and Straznicky, P. V., "Modelling of the Rivet Forming Process in Aluminum and Glare for Design Against Fatigue," *ICAF 2005*, EMAS, London, 2005.

[9] FEMB-PC, Finite Element Model Builder, Software Package, Ver. 27, Engineering Technology Associates, Inc., 2001.

[10] LS-DYNA Keyword User's Manual, Livermore Software Technology Corporation, 2003.

[11] DND, "MIL-HDBK-5H," 1998.

[12] de Rijck, R., "Stress Analysis of Fatigue Cracks in Mechanically Fastened Joints," Ph.D. Dissertation, Delft University of Technology, Delft, The Netherlands, 2005.

[13] Ball, D. L., "Elastic-Plastic Stress Analysis of Cold Expanded Fastener Holes," *Fatigue and Fracture of Engineering Materials and Structures*, Vol. 18, No. 1, 1995, pp. 47–63.

[14] Chang, J. B., "Prediction of Fatigue Crack Growth at Cold-Worked Fastener Holes," *Journal of Aircraft*, Vol. 14, No. 9, 1977, pp. 903–908.

[15] Hsu, Y. C., and Forman, R. G., "Elastic-Plastic Analysis of an Infinite Sheet Having a Circular Hole Under Pressure," *Journal of Applied Mechanics*, Vol. 42, No. 2, 1975, pp. 347–352.

[16] Rich, D. L., and Impellizzeri, L. F., "Fatigue Analysis of Cold-Worked and Interference Fit Fastener Holes," *Cyclic Stress-Strain and Plastic Deformation Aspects of Fatigue Crack Growth: A Symposium*, American Society for Testing and Materials, St. Louis, MO, 1976, pp. 153–175.

[17] Rans, C. D., Alderliesten, R. C., and Straznicky, P. V., "Residual Stresses in GLARE Laminates due to the Cold Expansion Process," *Proceedings of The Fifth Canadian International Composites Conference (CANCOM 2005)*.

[18] Li, G., Shi, G., and Bellinger, N. C., "Neutron Diffraction Measurement and FE Simulation of Residual Strains and Stress in Fuselage Lap Joints," Institute for Aerospace Research, Rept. LTR-SMPL-2004-0003, National Research Council of Canada, 2004.